Proceedings of 2024 IEEE
International Conference on Mechatronics and Automation
August 4 - 7, Tianjin, China

Design and Analysis of a Modular Flapping Wing Robot with a Swappable Powertrain Module

Snehit Gupta*, K P Rithwik, Kurva Prashanth, Avijit Ashe, Harikumar Kandath¶
Robotics Research Center - International Institute of Information Technology, Hyderabad
*snehit.g@research.iiit.ac.in, ¶harikumar.k@iiit.ac.in

***Abstract*—Flapping-wing robots (FWR) have domain-specific applications, where the lack of a fast-rotating propeller makes them safer when operating in complex environments with human proximity. However, most existing research in flapping-wing robots focuses on improving range/endurance or increasing payload capacity. This paper proposes a modular powertrain-based flapping-wing robot as a versatile solution to a mission-specific priority switch between payload or range for the same FWR. As the flapping frequency and stroke amplitude directly influence the flight characteristics of the FWR, we exploit this relation when designing our swappable powertrain with different motor-gearbox combinations and 4-bar crank lengths to obtain the desired frequency and amplitude. We calculate initial estimates for default configuration and simulate it using pterasoftware. We then fabricate two powertrain modules - a default configuration with a higher flapping frequency for payload purposes and an extended-range configuration with a tandem propeller for higher flight velocity for longer range and endurance. To verify the results, we compare the flight test data of both power train configurations using the same FWR platform.**

Video-https://youtu.be/vqJ58n77Bsc

***Index Terms*—Biomimetics, Flapping-Wing, Modular UAS**

I. Introduction

The field of bio-inspired robotics has seen a unique focus on developing flapping-wing robots that closely mimic the flight mechanics of birds and insects, aiming for advanced manoeuvrability and adaptability [1] [2]. A novel approach to bioinspired flapping wing UAV and its kinematic analysis involves the development of unique mechanisms for efficient flight [3]. In [4], the approach is to design a two-stage bionic flapping wing aircraft based on the physiological structure of large birds. Researchers have enhanced flight efficiency by analyzing the power consumption of components like motors, electronics, and vision systems [5]. Designing flapping-wing robots with long wingspans and efficient mass distribution enables extended flight times even with added payloads like vision modules [6]. The fuselage design focuses on reducing the aircraft's weight by employing a hollow middle and skinned outer layer, connected with a thick carbon fiber rod to ensure the relative position of each fuselage skeleton [7]. The development of servo-driven bird-like flapping-wing robots like USTBird-I incorporates a camber structure and a dihedral angle adjustment mechanism inspired by birds into its design and motion control of the wings [8].

Modular flapping wing robots have been a focus of research in recent years. Diez-de-los-Rios et al. propose a modular and re-configurable design for a flapping wing aerial robot consisting of Servo-Flapping Engine (SFE) modules for wing actuation, enabling control over amplitude, frequency, and phase for different flapping patterns [9]. This paper introduces RoboFalcon with a novel morphing-coupled wingbeat pattern for enhanced agility [10]. Moreno et al. present a hybrid fixed-flapping wing UAV that features an active roll wing deformation system to enhance the UAV's performance and durability [11]. Integrating these bio-inspired principles into robotics advances flight capabilities in versatile applications.

This paper describes a swappable powertrain-based FWR that can switch between payload and range configurations based on mission-specific requirements. The design process uses the fact that flapping frequency and stroke amplitude are related to the total take-off mass and flight velocity of the FWR. Two powertrain prototypes are fabricated, considering two different mission profiles. The default profile is meant for low flight speed, around 5 m/s, and can carry a payload of about 50 grams. The extended-range profile has a tandem propeller attached, enabling it to fly at a higher speed and leading to extended range. This is at the cost of a minimal increase in power consumption compared to the default configuration, as the required flapping frequency is reduced. The default profile has a higher flapping frequency than the extended-range one since all the thrust is generated only using flapping motion. Both profiles are flight-tested and proven to be stable. Critical parameters like flapping frequency, flight speed, power consumption, range, etc. are quantified from the flight test data. The results verify the utility of the swappable powertrain module for two different mission profiles.

II. Design Process

The flowchart presented in Fig. 1 describes our design process, which involves four steps - fixing initial requirements, estimating parameters, fabricating the prototype, and making the powertrain based on mission-specific requirements.

The initial requirement is fixed based on the required maximum take-off weight (MTOW), which includes the total mass of the FWR and the payload combined, represented by 'm', and in-flight cruise speed V. For a midsized FWR able to carry a small camera gimbal and ToF lidar, we estimated 50 gms of payload to be sufficient. Thus, the initial requirements for the default profile are fixed as follows:

- m = 400 gm (Maximum take-off mass)
- V = 5 m/s (Cruise Speed)

979-8-3503-8805-3/24/$31.00 ©2024 IEEE

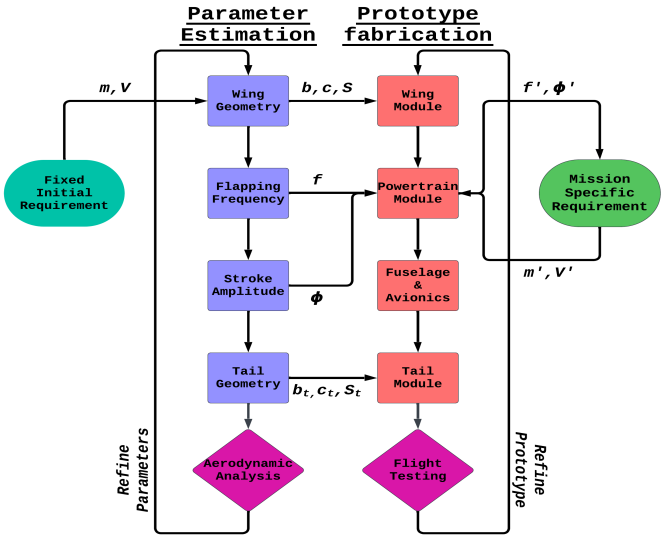

Fig. 1. Overview of the Design process

The mission-specific requirements m' and V' are satisfied by swapping the powertrain module with parameters f' and ϕ'.

TABLE I
SPECIFICATIONS

Parameter	Value	Description
m	400 gm	Mass (MTOW)
V	5 m/s	Cruise Speed
l	0.60 m	Overall Length
b	1.40 m	Wingspan
S	0.331 m^2	Wing Surface Area
c	0.30 m	Root Chord Wing
AR	5.92	Aspect Ratio
x_w	0.15 m	Wing-CG distance
b_t	0.35 m	Tailspan
S_t	0.066 m^2	Tail Surface Area
c_t	0.25 m	Root Chord Tail
x_t	0.35 m	CG-Tail distance
θ	15 deg	Elevator pitch
ϕ	52.5 deg	Flapping amplitude
f	3.2 Hz	Flapping frequency
D	6 deg	Mean dihedral
α	10 deg	Angle of Attack
ρ	1.225 kg/m^3	Air Density
g	9.81 m/s^2	Gravity

III. Estimation of Parameters

Before fabricating the FWR prototype, we estimate the parameters that determine the flight characteristics of our FWR based on the initial requirements. We estimate dimensional parameters derived from the 2D wing and tail geometry design, such as wingspan and chord length. Other parameters, such as flapping frequency and stroke amplitude, are calculated mathematically. Aerodynamic simulation of Forces and Moments is performed using the pterasoftware [12], and we iteratively refine the model parameters based on the inputs to attain the desired outputs. These parameters and the initial requirements together make the default specifications of FWR used for the fabrication process (Table I).

A. Wing Geometry

An elliptical-shaped wing was preferred to reduce wing tip loss and increase agility at low speeds [13]. We chose a medium-sized wingspan of 1400 mm and a root chord length of 300mm, allowing the FWR to be man-portable when folded. While designing the 2D wing geometry, the ellipse was slightly modified to extend outwards near wing tips to have a larger flexible area to generate more forward thrust and lift by wing tip vortexes, as shown in Fig. 5.

B. Flapping Frequency

The flapping frequency is related to the total mass and wing dimensions, which is estimated using Hassanalian's methodology [14]. The correction factor ζ is approximated around 1.5 based on data from a similar-sized FWR [15]. The frequency 'f' calculated from the input parameters equals 3.2257 Hz using (1).

$$f = \zeta m^{\frac{3}{8}} g^{\frac{1}{2}} b^{-\frac{23}{24}} S^{-\frac{1}{3}} \rho^{-\frac{3}{8}} \tag{1}$$

C. Stroke Amplitude

The flapping angle domain 'ha' is calculated based on the Strouhal number St, which is set equal to 0.4 [14]. The upstroke and downstroke angles are symmetric from the mean dihedral position D. The half stroke amplitude '$\frac{\phi}{2}$' was estimated to be around 26.2873 deg using (2). The stroke amplitude ϕ is rounded to 52.5 deg.

$$\frac{\phi}{2} = \sin^{-1}\left(\frac{2ha}{b}\right), St = \frac{2fha}{V} \tag{2}$$

D. Tail Geometry

The tail geometry is designed in a way that satisfies (3) (4). The centre of gravity (CG) is assumed to be 0.5 wing root chord length from the leading edge.

$$\frac{mg}{\frac{1}{2}\rho V^2 S} = 2\pi \frac{AR}{AR+2}\alpha + \frac{\pi}{2}\alpha + \frac{\theta b_t^2}{t} \tag{3}$$

$$4\frac{AR}{AR+2}\frac{x_w}{c} - \frac{b_t^2}{S}\frac{x_t}{c} = 0, AR = \frac{b^2}{S} \tag{4}$$

E. Aerodynamics Analysis

We use pterasoftware [12] "unsteady ring vortex lattice method solver" to estimate approximate forces and moments acting on the FWR as shown in Fig. 2 and Fig. 3. A flat airfoil NACA 0000 was chosen, and α was set to 10 deg. After a cyclic process of fine-tuning the inputs to the solver, the simulation satisfied the desired outputs. Table II has the solver output values with the known input parameters.

TABLE II
AVERAGED FORCES AND MOMENTS

Description	Symbol	Value
Lift	L	4.941 N
Induced Drag	D_i	1.912 N
Lateral Force	Y	0.0 N
Rolling Moment	L_{roll}	0.0 Nm
Pitching Moment	M_{pitch}	-0.326 Nm
Yawing Moment	N_{yaw}	0.0 Nm

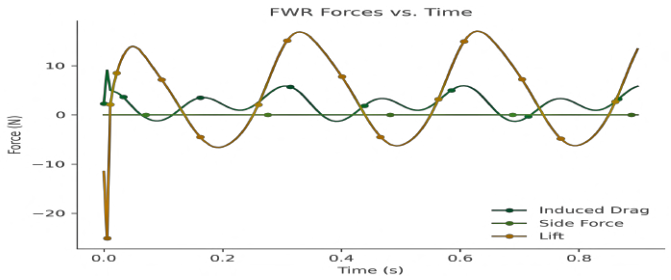

Fig. 2. forces vs time over three flap cycles

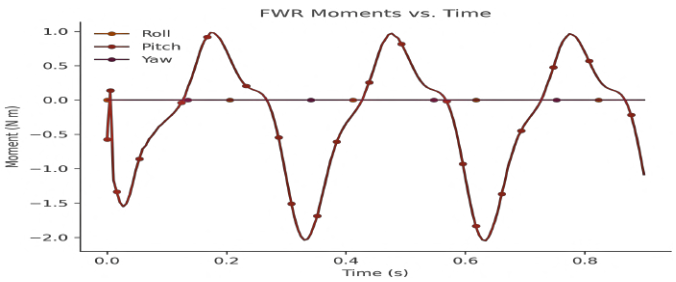

Fig. 3. moments vs time over three flap cycles

IV. Prototype Fabrication

As the next step in the design process, the fabrication process involved building the prototype around the earlier specified parameters. The modular design lets us quickly assemble the entire FWR using four modules - powertrain, wing, fuselage and tail (Fig. 4). Most of the modules went under roughly three stages of refinement.

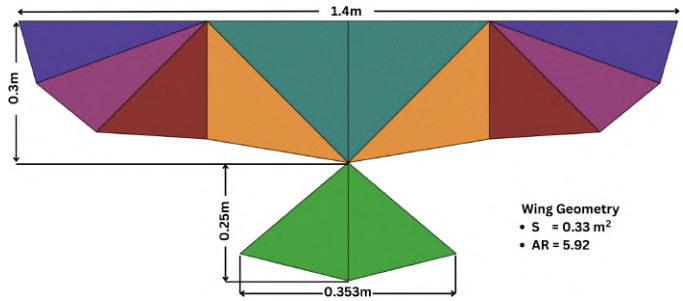

Fig. 5. Wing Geometry

A. Thin Membrane Wing

It is crucial to build the wing as light as possible while being durable at the same time. Lower wing inertia reduces the torque required for flapping, using less power. To achieve this, a thin membrane-based wing with flexible ribs was selected. The wing membrane uses a 50-micron cellophane sheet with pultruded carbon rods as the ribs, held together by a PLA 3D-printed elbow fixture. The entire wing weighs under 65 grams. We went ahead with a flat wing due to the ease of fabrication, lighter weight and higher durability during rough landings.

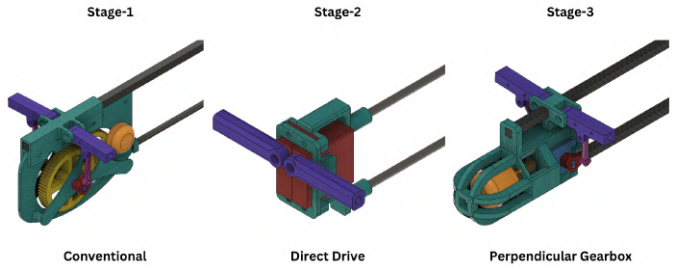

Fig. 6. stages of powertrain development

B. Swappable Powertrain

Looking at the current state-of-the-art flapping wing robots, the common feature about most was a conventional, exposed spur gear powertrain. Although simple and easy to build, this design was rejected due to space constraints and lack of modularity. The next step was using a direct drive independent servo actuated powertrain. This has significant advantages over the existing designs in terms of lighter weight, compact size, and no tail control needed due to independent amplitude and dihedral control. However, the maximum flapping frequency is limited; it must be high enough to carry any substantial weight. Thus, flight speed is low compared to the previous module. It can be more useful in indoor designs because it is much more compact, and slow flapping makes it safer for humans in complex environments. However, for our purpose, we found out it cannot reach the desired high flapping frequencies that a geared-down motor can provide. Fig. 6 shows the powertrain module CAD models in the development process.

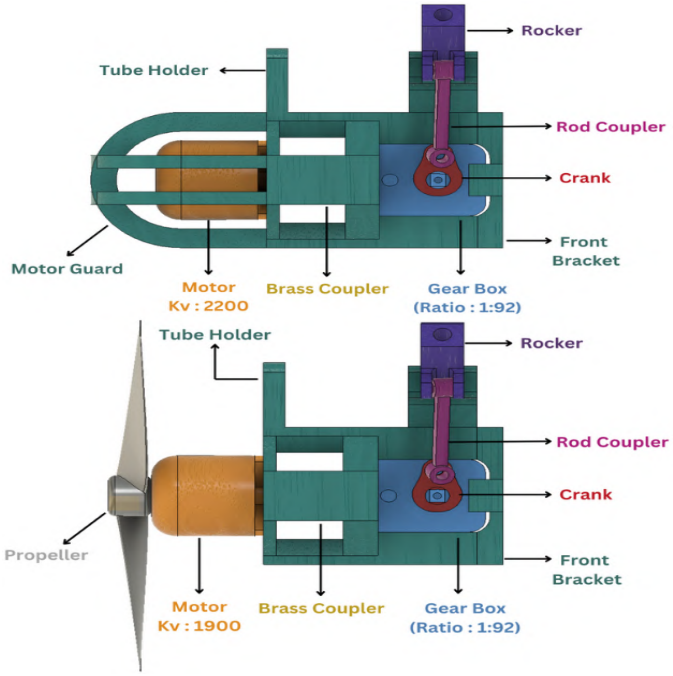

Fig. 7. default powertrain (up) and extended-range powertrain (down)

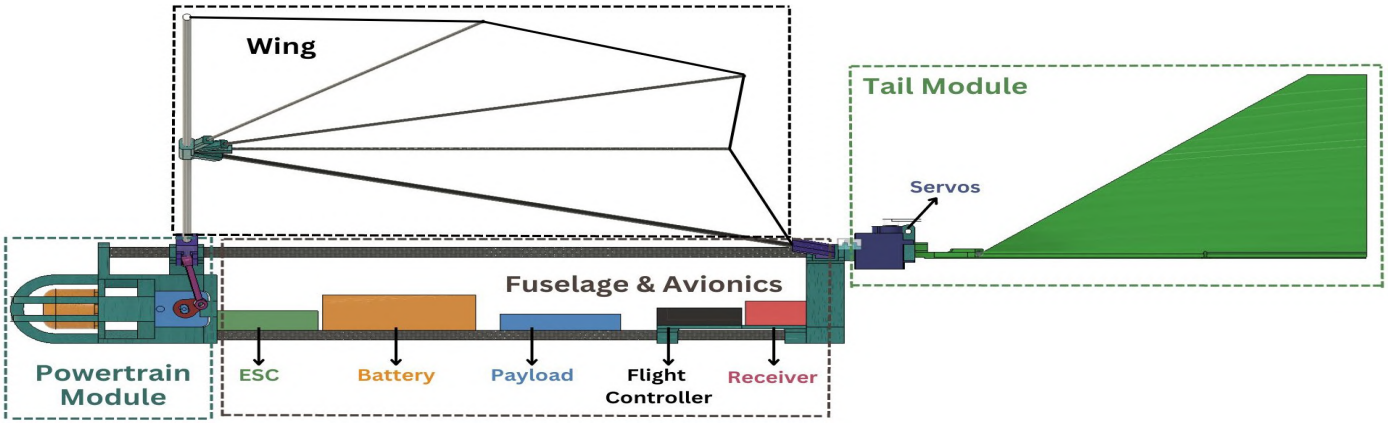

Fig. 4. Schematic diagram of the FWR from the CAD model

The final module design is compact and lightweight, with enough power to achieve high flapping frequencies under load. It uses an off-the-shelf 1:92 metal TT motor gearbox attached in bevel alignment. This powertrain module uses a 4-bar mechanism to generate the flapping motion. The swappable motor gearbox mount is 3D-printed using PLA; the crank is CNC-milled aluminium, and the coupler uses M3 ball socket joints in a perpendicular phase between the rocker and crank motions. The flapping amplitude with the 4-bar mechanism is limited to 52 degrees, +26 and -26 degrees from a dihedral angle of 6 deg.

The default drivetrain module (Fig. 7) utilizes an AT-2306 2200 Kv BLDC motor with a high power-to-weight ratio, delivering 230 watts of power with an effective flapping frequency of around 3-5 Hz. For our extended-range configuration (Fig. 7), we employ an AT-2306 1900 Kv BLDC motor generating 140 watts of max power with an effective flapping frequency of around 2-3 Hz. The lower thrust due to reduced flapping frequency in the extended-range module is compensated using a tandem propeller. We maintain the original stroke amplitude for comparison. However, it can also be adjusted using a different-length crank in our 4-bar mechanism.

TABLE III
MODULE CONFIGURATION

Powertrain	Default	Extended-Range
Motor	2200 Kv	1900 Kv
ESC	30 A	30 A
Battery	3S - 1000 mAh	2S - 2250 mAH
Frequency	3-5 Hz	2-3 Hz
Amplitude	52 deg	52 deg
Propellor	N/A	6x4

C. Tail Module

We fabricated three types of tail modules - D-tail, V-tail, and C-tail, as shown in Fig. 8 [16]. We individually tested each of them in flight to assess control responsiveness. D-tail, utilizing ladder rotation, posed significant challenges for lateral manoeuvring. Subsequently, we experimented with the inverted V-tail with 3 DoF through elevon mixing of ventral fins and rudder. The elevator and rudder control was satisfactory. However, we identified poor responsiveness in aileron control due to high wing inertia and low torque generated by control surfaces, being too close to the roll axis.

Ultimately, we reverted to a conventional tail due to its simplicity and effectiveness. The tail module comprises a kite-shaped structure made of depron and carbon rods for structural reinforcement. The large, full-moving control surfaces enable high agility and angle of attack, even at very low speeds. Two 9 gm metal gear SG-90 servos operate the elevator and rudder movement.

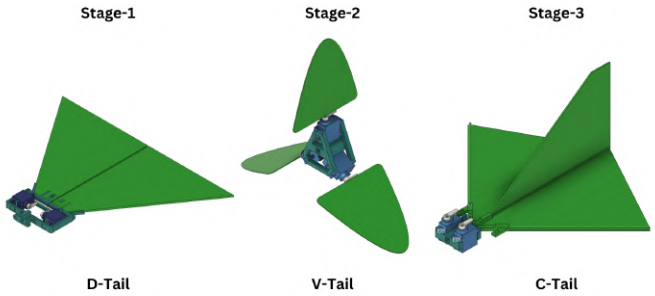

Fig. 8. stages of tail development

D. Fuselage and Avionics

The fuselage is a barebone structure that keeps weight at a minimum while being strong enough to hold everything together. Two parallel square carbon tubes are held together using a PLA fixture. The design allows for a quick swap of modules by just sliding them in place on the upper tubes. The electronics and payload are mounted on a sliding tray on the bottom tube to quickly adjust the centre of gravity when using a different battery or payload.

We chose standard off-the-shelf available electronics for the prototype for quick and easy assembly. Holybro Kakute H7V2 - STM32H743 was the preferred flight controller, weighing 8

grams. Open-source autopilot INAV 7 runs onboard the flight controller for data logging and control. A 30 amp ESC controls the BLDC motor. The default battery used is 3S-1000 mAh-40C Li-Po to power the electronics, providing 40 amps of continuous discharge current, exceeding the maximum current required by the motor. The range-optimised configuration uses a higher capacity 2S-2250 mAh-15C Li-Ion to enhance flight endurance with a discharge rate of 33.5 A / 67 A (Table III).

V. Experiments and Results

To test the flight performance of the FWR prototype, we flew the FWR in both powertrain configurations one by one. After doing a few glide tests to adjust the centre of gravity by shifting battery position, tests were done in almost identical conditions in the open by hand launching them in mild wind, around 600m above sea level. We manually controlled the FWR using the Transmitter, observed the flight characteristics response based on the input, and recorded the IMU and GPS logs onboard the black box. 50 gm dummy payload was attached to the default profile, while the range-extended one has a 6x4 tandem propeller attached instead. The Table IV compares the two configurations.

TABLE IV
Performance Comparison

Profile	Default	Extended-Range
Mass w/o payload	398 gm	422 gm
Payload	50 gm	N/A
Amplitude	52 deg	52 deg
Frequency	4.5 Hz	2 Hz
Cruise Speed	5.2 m/s	7.7 m/s
Current drawn	6.2 A	7.7 A
Endurance*(estimated)	9 mins	17 mins
Range*(estimated)	2.8 km	7.8 km

A. Profile-1 (default)

The graphs presented represent an 8-second window of flight data while cruising. As observed in Fig. 9, the attitude of the FWR shows that the pitch angle (theta) during mid-flight is relatively high and close to 30 deg. The roll angle (phi) is close to zero with slight variation based on coupled response to rudder control; Yaw movement is observed changing (psi) towards one side based on rudder control. Finally, the accelerometer log in Fig. 10 shows the FWR's flapping frequency around 4.5 hz.

The mean flight velocity (Fig. 11) from GPS data was around 5.2 m/s, close to our initial requirement of 5 m/s cruise speed. The mean current drawn is measured to be 6.2 A, resulting in a theoretical endurance of 9 minutes using the 3S-1000 mAH battery. Thus, the maximum range at 5.2 m/s cruise speed would be around 2.8 km.

We also tried using a 2600 Kv motor with this configuration for a higher payload. However, the practical limitations of increased flapping frequency make it mechanically inefficient due to extreme drag forces acting on the wing.

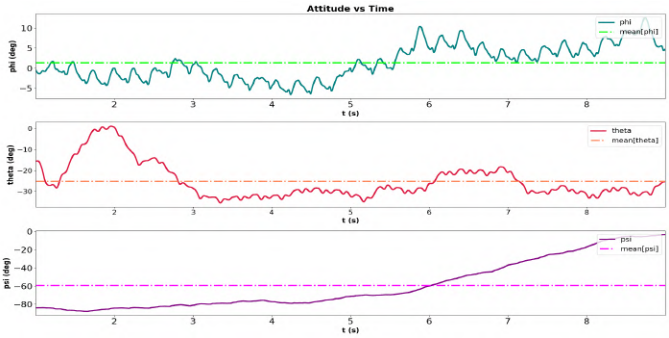

Fig. 9. Attitude log of profile-1

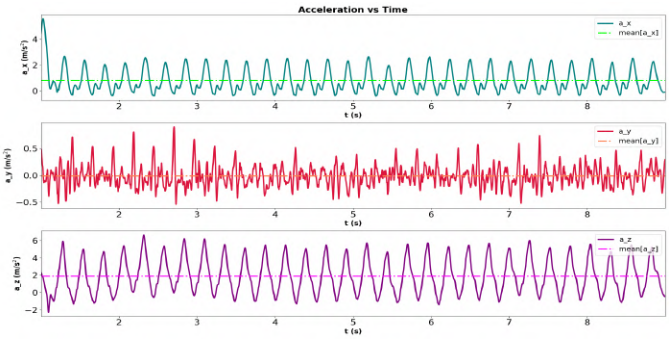

Fig. 10. Accelerometer log of profile-1

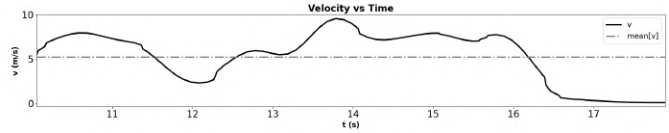

Fig. 11. GPS velocity log of profile-1

B. Profile-2 (extended-range)

The graphs presented represent an 8-second window of flight data while cruising. Again, as observed in Fig. 12, the attitude of the FWR shows that the pitch (theta) during mid-flight is close to 20 deg. The roll angle (phi) is non-zero due to a constant coupled response to rudder control; the yaw angle has a discontinuity where the scale switches from -360 to 0 in (psi). The accelerometer log in Fig. 13 shows the FWR's flapping frequency roughly around 2 hz.

The mean flight velocity (Fig. 14) from GPS data was around 7.7 m/s, which is roughly 50 percent higher than our default profile. The mean current drawn is measured to be 7.7 A, resulting in a theoretical endurance of 17 minutes using the 2S-2250 mAH battery. Thus, the maximum range at 7.7 m/s would be around 7.8 km.

The propeller can be swapped for a larger diameter for more thrust. However, the flight characteristics become closer to that of a fixed-wing than a FWR at higher throttles, so a clutch mechanism is required to switch modes like a Hybrid UAV.

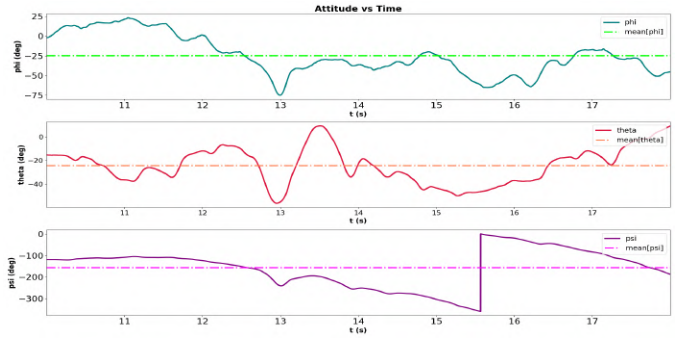

Fig. 12. Attitude log of profile-2

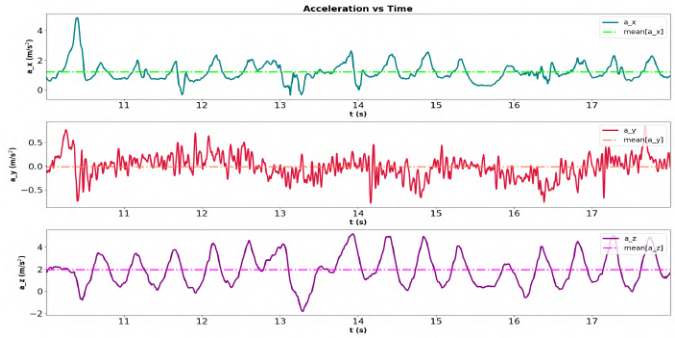

Fig. 13. Accelerometer log of profile-2

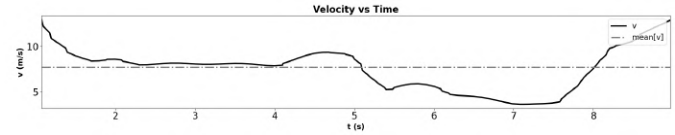

Fig. 14. GPS velocity log of profile-2

VI. Conclusion

This paper presents a modular flapping wing robot design with a swappable powertrain, which can be changed to mission-specific requirements and aims to increase the application domain of flapping wing robots. The prototype was fabricated based on the initial requirements set, and two powertrain configurations were built. We performed multiple flight tests to refine the prototype in stages and analysed the experimental data. The flight tests support achieving mission-specific requirements by swapping the powertrain module.

However, there are limitations to what this FWR can achieve just by changing flapping frequency and stroke amplitude, as a longer wingspan would be required for payload capacities of more than a hundred grams to be effective. This is due to the limited range of frequencies and amplitude that is practically possible, as the drag required increases exponentially on an increasing frequency, and the maximum amplitude is a limited angle less than π radians.

Future work includes collaboration on using dielectric elastomer actuators (DEA) as artificial muscles to create a flapping motion more efficiently than a mechanical motor-driven 4-bar mechanism on a smaller-scale prototype.

Acknowledgement

The authors acknowledge the support provided by MeitY, Govt. of India, under the project "Capacity Building for Human Resource Development in Unmanned Aircraft System (Drone and Related Technology)."

References

[1] Jae-Hung, Han., Yu, Han., Hyeon-Ho, Yang., Sang-Gil, Lee. (2023). A Review of Flapping Mechanisms for Avian-Inspired Flapping-Wing Air Vehicles. Aerospace, doi: 10.3390/aerospace10060554

[2] Sakito, Koizumi., Toshiyuki, Nakata., Hao, Liu. (2023). Development of a flapping mechanism inspired by the flexible wing-base structure of insects for wing motion control. Journal of Biomechanical Science and Engineering, doi: 10.1299/jbse.22-00347

[3] Dewangan B, Pradhan D, Roy H. Bioinspired flapping wing UAV and its kinematic analysis—a novel approach. Proceedings of the Institution of Mechanical Engineers, Part K: Journal of Multi-body Dynamics. 2022;236(4):570-587. doi:10.1177/14644193221113664

[4] Fu, Xiaokun, Hao, Yongping, Ma, Minghui, Zheng, Xuyang. (2023). Design and Analysis of A Two-stage Bionic Flapping Wing Aircraft. Journal of Physics: Conference Series. 2528. 012055. 10.1088/1742-6596/2528/1/012055.

[5] Tapia, Raul, Alvaro Cesar Satue, Saeed Rafee Nekoo, José Ramiro Martínez-de Dios, and Anibal Ollero. "Experimental Energy Consumption Analysis of a Flapping-Wing Robot." arXiv, June 1, 2023. https://doi.org/10.48550/arXiv.2306.00848.

[6] Wu, Xiaoyang, Wei He, Qiang Wang, Tingting Meng, Xiuyu He, and Qiang Fu. "A Long-Endurance Flapping-Wing Robot Based on Mass Distribution and Energy Consumption Method." IEEE Transactions on Industrial Electronics 70, no. 8 (August 2023): 8215–24. https://doi.org/10.1109/TIE.2022.3213905.

[7] Yunde Shi, Wang He, Mingqiu Guo, Dan Xia, Xiang Luo, Xiaoqiang Ji, "Mechanism Design and Motion Analysis of a Flapping-Wing Air Vehicle", Mathematical Problems in Engineering, vol. 2022, Article ID 7920914, 11 pages, 2022. https://doi.org/10.1155/2022/7920914

[8] Huang, Haifeng, He, Wei, Fu, Qiang, He, Xiuyu, Sun, Changyin. (2022). A Bio-Inspired Flapping-Wing Robot With Cambered Wings and Its Application in Autonomous Airdrop. IEEE/CAA Journal of Automatica Sinica. 9. 2138-2150. 10.1109/JAS.2022.106040.

[9] Diez-de-los-Rios, Ivan, Suárez, Alejandro, Sanchez-Laulhe, Ernesto, Armengol, Inmaculada, Ollero, Anibal. (2021). Winged Aerial Robot: Modular Design Approach. 190-195. 10.1109/SSRR53300.2021.9597868.

[10] A. Chen, B. Song, Z. Wang, D. Xue and K. Liu, "A Novel Actuation Strategy for an Agile Bioinspired FWAV Performing a Morphing-Coupled Wingbeat Pattern". 10.1109/TRO.2022.3189812.

[11] Moreno, J., Ruiz, Cristina, Satue, Alvaro, Acosta, J. Á, Ollero, Anibal. (2022). Design, development and testing of a Hybrid Fixed-Flapping wing UAV. 329-338. 10.1109/ICUAS54217.2022.9836114.

[12] Urban, Cameron, Agarwal, Ramesh. (2022). Validation and Optimization of Ptera Software: An Open-Source Unsteady Flow Simulator for Flapping Wings. 10.2514/6.2022-1967.

[13] Liu, Dan, Song, Bifeng Yang, Wenqing Yang, Xiaojun Xue, Dong Lang, Xinyu. (2021). A Brief Review on Aerodynamic Performance of Wingtip Slots and Research Prospect. Journal of Bionic Engineering. 18. 10.1007/s42235-021-00116-6.

[14] M. Hassanalian, A. Abdelkefi, M. Wei, and S. Ziaei-Rad, "A novel methodology for wing sizing of bio-inspired flapping wing micro air vehicles: Theory and prototype," Acta Mech., vol. 228, no. 3, pp. 1097–1113, 2017.

[15] R. Zufferey et al., "Design of the High-Payload Flapping Wing Robot E-Flap," in IEEE Robotics and Automation Letters, vol. 6, no. 2, pp.3097-3104, April 2021, doi: 10.1109/LRA.2021.3061373.

[16] M. Guzmán et al., "Design and comparison of tails for bird-scale flappingwing robots," in Proc. IEEE/RSJ Int. Conf. Intell. Robots Syst., 2021, pp. 6358–6365.